Supporting Information for "Interparticle torques suppress motility-induced phase separation for rodlike particles"

Robin van Damme[1], Jeroen Rodenburg[2], René van Roij[2], and Marjolein Dijkstra[1]
[1] *Soft Condensed Matter, Debye Institute for Nanomaterials Science, Utrecht University, Princetonplein 1, 3584 CC Utrecht, The Netherlands*
[2] *Institute for Theoretical Physics, Utrecht University, Princetonplein 5, 3584 CC Utrecht, The Netherlands*
(Dated: March 14, 2019)

S1. INSIGNIFICANCE OF EFFECTIVE TRANSLATIONAL DIFFUSION

In the stability analysis we have mapped the effect of interparticle forces into an effective swim speed v^{eff} and an effective translational diffusion D_t^{eff}. Previous literature with similar stability analyses has assumed that this effective translational diffusion is equal to the bare translational diffusion i.e. $D_t^{\text{eff}} = D_t$, usually as an approximation or closure [1, 2]. We opted to check this whether such an assumption is reasonable for 3D spheres and rods as well by measuring it from the 3D mean square displacement (MSD)

$$\langle |\boldsymbol{r}_i(t) - \boldsymbol{r}_i(0)|^2 \rangle = \frac{(v^{\text{eff}})^2}{2(D_r^{\text{eff}})^2}\left(e^{-2D_r^{\text{eff}}t} - 1\right) + 6\left(D_t^{\text{eff}} + \frac{(v^{\text{eff}})^2}{6D_r^{\text{eff}}}\right)t. \tag{S1}$$

Similar to Ref. [2], we associate D_t^{eff} with the long-time diffusion constant of a passive system. For a passive system, the MSD becomes

$$\langle |\boldsymbol{r}_i(t) - \boldsymbol{r}_i(0)|^2 \rangle = 6D_t^{\text{eff}}t. \tag{S2}$$

Figure S1 shows the MSD measured for a system of passive spheres at a packing fraction of $\phi = \pi\sigma^3 N/6V = 0.3$. At short times, diffusion is essentially free and $D_t^{\text{eff}} = D_t$. At long times the particle interactions lead to an effective decrease of the diffusion coefficient. This decrease depends on the density of the system. For $\phi = 0.3$, we find that $D_t^{\text{eff}}/D_t \approx 0.34$. While this decrease is significant in terms of the diffusion of passive particles, it is entirely *in*significant when considering the stability of the homogeneous isotropic phase for self-propelled particles, as long as the Péclet number is higher than roughly Pe ~ 1. Thus, we just approximate $D_t^{\text{eff}} = D_t$.

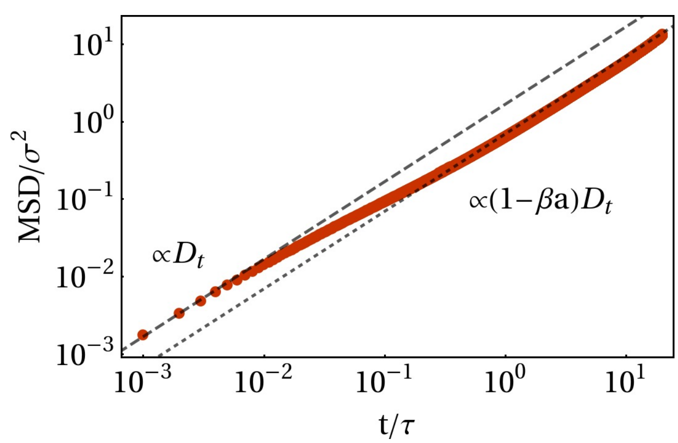

Figure S1: Mean square displacement of $N = 200$ 3D passive spheres (Pe = 0) at a packing fraction of $\phi = 0.3$. At very small times, there is free diffusion i.e. MSD/$\sigma^2 \approx 6D_t t$, while at long times the particle interactions lead to a decrease of the diffusion coefficient i.e. MSD/$\sigma^2 \approx 6D_t^{\text{eff}}t$.

S2. HYDRODYNAMICS FRICTION COEFFICIENTS FOR 3D SPHEROCYLINDRICAL PARTICLES

In Figure S2 we show the hydrodynamic friction factors of short ($1 \leq l/\sigma < 2.5$) spherocylinders and ellipsoids in 3D, defined with respect to a sphere of the same volume as detailed in Ref. [3]. For these aspect ratios the difference between ellipsoids and spherocylinders is minimal, so one can safely use the exact friction factors that were determined by Perrin in Ref. [4].

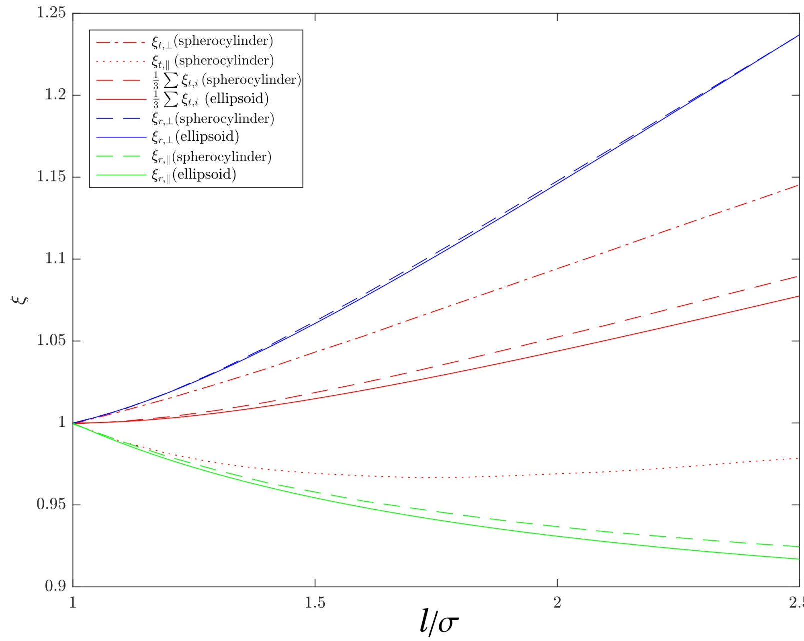

Figure S2: Hydrodynamic friction coefficients for ellipsoids and spherocylinders for small aspect ratios $1 < l/\sigma < 2.5$, defined with respect to a sphere of the same volume [3]. The red long-short dashed and dotted lines indicate the translational friction coefficients of spherocylinders, while the red solid and dashed lines indicate the total friction coefficient of ellipsoids and spherocylinders, respectively. The green and blue lines indicate the rotational friction coefficients around and perpendicular to the long axis, respectively. The difference between any of the curves in this aspect ratio regime are $< 5\%$, so we can safely approximate the translational and rotational friction coefficients of spherocylinders by those of ellipsoids.

S3. FINITE-SIZE EFFECTS WHEN MEASURING EFFECTIVE SWIM SPEED AND ROTATIONAL DIFFUSION

Measuring the effective swim speed v^{eff} and rotational diffusion D_r^{eff} from simulations with only few particles ($N \sim 100$) means these constants will suffer from finite-size effects. Here we show the magnitude of this effect. Figure S3 shows the scaling of (a) the effective swim speed v^{eff} and (b) the fraction of particles in the largest cluster f_{cl} with the inverse of the number of particles N for 3D active spheres, at a packing fraction $\phi = 0.44$ and a Péclet number of $\text{Pe} = 100$. A clear kink can be seen in both graphs at roughly the same system size ($N \sim 4000$), which after visual inspection of the corresponding snapshots (Fig. S4) can be associated with MIPS. As our small-N simulations take place well below this threshold and v^{eff} does not scale strongly with the number of particles in this regime, we assume that they provide a reasonable estimate of the effective swim speed even when a larger system would phase-separate.

S4. ADDITIONAL SIMULATION SNAPSHOTS

[1] J. Bialké, H. Löwen, and T. Speck, EPL **103**, 30008 (2013), arXiv:1307.4908.
[2] T. Speck, A. M. Menzel, J. Bialké, and H. Löwen, J. Chem. Phys. **142**, 224109 (2015), arXiv:1503.08412.
[3] B. Bet, G. Boosten, M. Dijkstra, and R. van Roij, J. Chem. Phys. **146**, 084904 (2017), arXiv:1603.02629.
[4] F. Perrin, J. Phys. Radium **5**, 497 (1934).

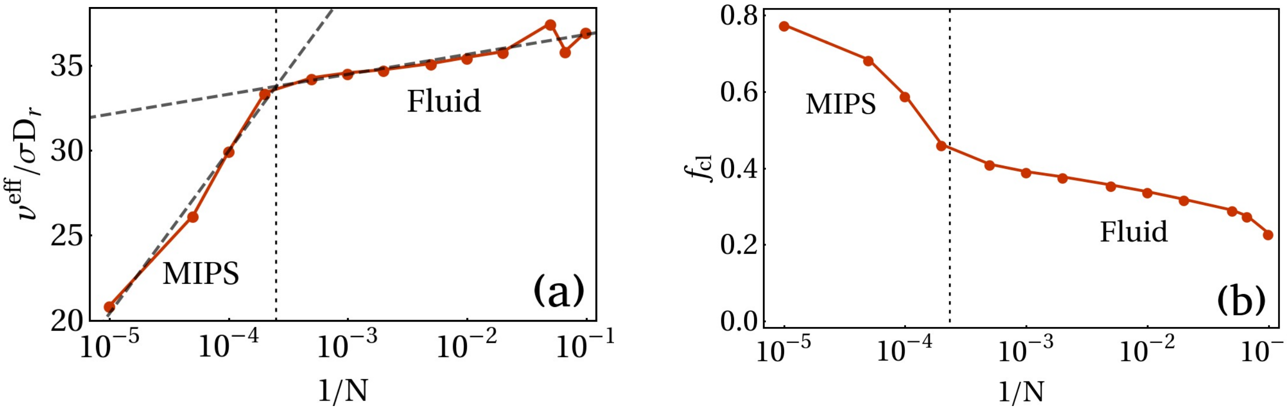

Figure S3: Effective swim speed $v^{\rm eff}$ (a) and fraction of particles in the largest cluster f_{cl} (b) for 3D active spheres as a function of the inverse of the number of particles N, at a packing fraction $\phi = 0.44$ and a Péclet number of $\mathrm{Pe} = 100$. Both $v^{\rm eff}$ and $f_{\rm cl}$ display a clear kink around $N \sim 4000$ that denotes MIPS. The dashed lines are drawn to show the transition in scaling from the fluid to the MIPS regime, and the dotted line denotes the intercept at $N \approx 4000$.

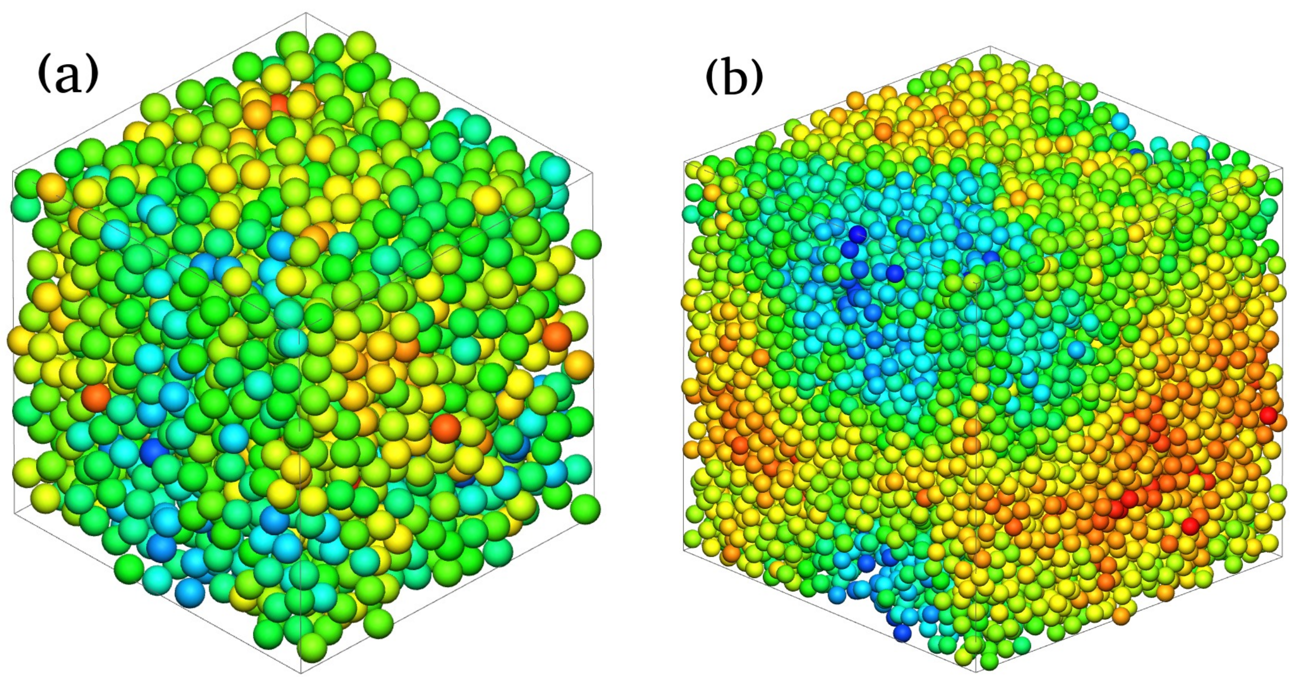

Figure S4: Two representative snapshots of the simulated system of Fig. S3 for (a) $N = 2000$ in the fluid regime, and (b) $N = 10000$ in the MIPS regime. Particles are coloured according to their local density. While no large-scale phase separation can be seen for (a), (b) has clearly separated into a dense and a dilute region.

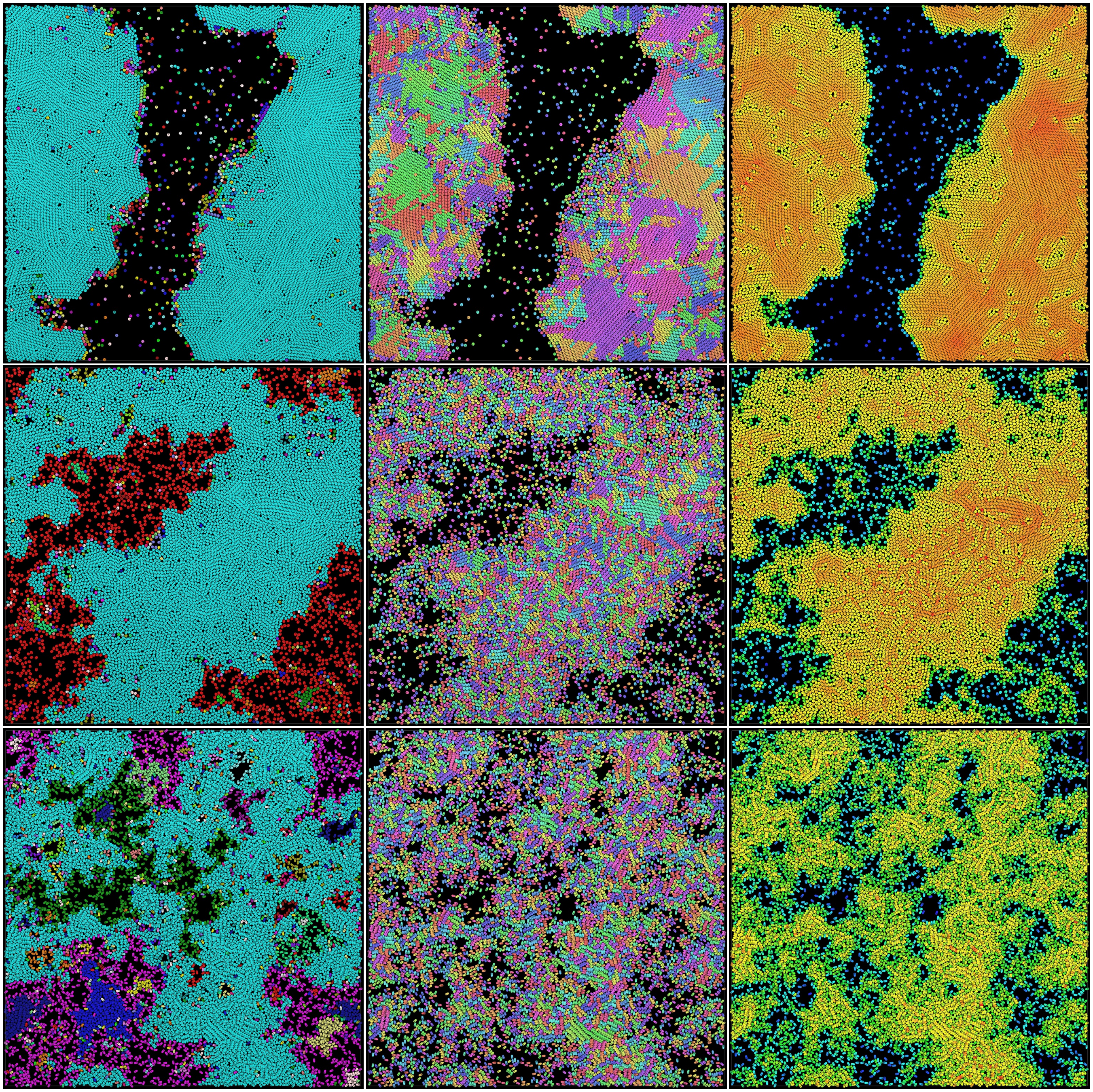

Figure S5: 2D Simulation snapshots for $N = 10000$ rods with aspect ratios $l/\sigma = 1.1$ (top), $l/\sigma = 1.3$ (top) and $l/\sigma = 2.0$ (bottom), at $\phi = 0.6$, $\mathrm{Pe} = 100$, deep within the MIPS region. The columns depict the same snapshot three times with various color maps. The left column shows the distribution of clusters, where each cluster is assigned a unique color. In the middle column the color is indicative of the particle orientation, with nematic symmetry. Zooming in also shows black stripes that indicate the polar orientations. In the right column the color represents the local density. Even though all three snapshots show a separation into dense and dilute regions, form a single connected cluster and have no global orientational order (and are thus classified as MIPS), the three cases are clearly different.